

# In-Context Operator Learning for Linear Propagator Models

Tingwei Meng\*    Moritz Voss\*<sup>†</sup>    Nils Detering<sup>‡</sup>  
 Giulio Farolfi\*    Stanley Osher\*    Georg Menz\*

January 28, 2025

## Abstract

We study operator learning in the context of linear propagator models for optimal order execution problems with transient price impact à la Bouchaud et al. (2004) and Gatheral (2010). Transient price impact persists and decays over time according to some propagator kernel. Specifically, we propose to use In-Context Operator Networks (ICON), a novel transformer-based neural network architecture introduced by Yang et al. (2023), which facilitates data-driven learning of operators by merging offline pre-training with an online few-shot prompting inference. First, we train ICON to learn the operator from various propagator models that maps the trading rate to the induced transient price impact. The inference step is then based on in-context prediction, where ICON is presented only with a few examples. We illustrate that ICON is capable of accurately inferring the underlying price impact model from the data prompts, even with propagator kernels not seen in the training data. In a second step, we employ the pre-trained ICON model provided with context as a surrogate operator in solving an optimal order execution problem via a neural network control policy, and demonstrate that the exact optimal execution strategies from Abi Jaber and Neuman (2022) for the models generating the context are correctly retrieved. Our introduced methodology is very general, offering a new approach to solving optimal stochastic control problems with unknown state dynamics, inferred data-efficiently from a limited number of examples by leveraging the few-shot and transfer learning capabilities of transformer networks.

## 1 Introduction

Devising optimal order execution strategies for buying or selling large volumes of shares of a stock on a centralized exchange is a major concern for large institutional investors and hence became a well-studied problem in financial mathematics in the past two decades. The aim is to split up a large meta order into smaller child orders which are executed over some time horizon to mitigate adverse price impact incurred by large trades. We refer to the excellent monographs [CJP15, Gué16, BBDG18, Web23] for a comprehensive overview of this topic.

This paper addresses an optimal liquidation problem in the context of linear propagator models proposed by [BGPW04, BFL09, Gat10]. Propagator models constitute a versatile class of transient price impact models, defined by a price impact kernel (propagator), which reliably captures in reduced form the interplay between price moves and current and past trades as empirically observed when executing market orders in limit order books. The tractability of linear propagator models also provides a convenient framework for formulating optimal

---

\*University of California Los Angeles, Department of Mathematics, Los Angeles, CA 90095, USA.

<sup>†</sup>Corresponding author.

<sup>‡</sup>Heinrich Heine University Düsseldorf, Mathematisches Institut, Universitätsstraße 1, 40225 Düsseldorf, Germany.

execution problems as stochastic optimal control problems, which have recently been solved in full generality by [AJN22] for a wide range of different propagator kernels. In contrast, our approach is concerned with the limitations of postulating a specific parametric propagator model in real-world trading applications, where market conditions are non-stationary and vary over time, and stylized price impact parameters capturing the interaction with the market when executing trades are difficult to estimate in a reliable and persistent manner. In fact, financial markets can be likened to quantum systems, where every interaction leaves a trace and alters the conditions. Therefore, minimizing interference is crucial when inferring their current state from observations. This particularly applies to assessing the price impact of trading. To tackle this challenge, we propose a novel in-context operator learning framework, termed ICON-OCnet. Specifically, we adapt the In-Context Operator Networks (ICON) learning methodology proposed in [YLMO23] to (i) learn the *unknown* price impact prevailing in a *current* market environment from only a few recent executed or observed trades, and then (ii) devise the associated optimal order execution strategy, a neural network optimal control policy (called OCnet), for the detected price impact regime. We examine this general idea within the broad class of linear propagator models with various price impact kernels, where we can effectively benchmark our methodology against the ground truth optimal execution strategies obtained in [AJN22]. We also provide an alternative representation of the optimal solution by using the more direct approach and results from [AJNV23], which might be of independent interest.

Our proposed ICON-OCnet method is based on an *in-context learning paradigm*, in other words, (transfer-)learning from prompted examples (context). To this end, we leverage a transformer-based architecture. The idea is to infer the price impact operator which maps the trading rate to the incurred price impact only from few observed examples, allowing the transformer to adjust to new or unseen price impact models without requiring full retraining of the network. First, we train the ICON model offline on synthetically generated trade and price impact trajectories from a wide range of propagator model specifications. The pre-trained ICON model is then initialized with only a few examples of trades and corresponding price impact in order to infer in a few-shot online learning manner the underlying propagator model from the prompted context. In a second step, we feed the initialized ICON model as a surrogate operator into the optimal order execution problem and train a neural network policy via a policy gradient method akin to [HE16] to learn the optimal execution strategy for the price impact operator inferred by ICON from the provided context. We validate the performance of our ICON-OCnet approach through various numerical experiments, demonstrating its ability to (i) detect the true price impact operator even when trained on data from a different propagator model class, and to (ii) correctly recover the corresponding optimal order execution strategy from the propagator model generating the in-context examples. In particular, the ICON surrogate operator demonstrates sufficient precision and robustness to be effectively utilized in an iterative stochastic gradient descent-type optimization algorithm to learn corresponding optimal policies.

Finally, the broader purpose of this paper is also to demonstrate a *proof of concept* for our general methodology in a complex and non-trivial setting: solving a non-Markovian optimal control problem with unknown state dynamics, inferred in a data-efficient and robust manner from a limited number of in-context examples by bringing to bear the few-shot and transfer learning capacities of transformer networks.

Closely related to our work, in the sense of addressing a similar problem, are [NZ23] and [NSZ23]: [NZ23] introduces a statistical online learning approach for linear propagator models, alternating between exploration and exploitation phases, and achieving sublinear regret with high probability; [NSZ23] proposes an offline learning framework to estimate the price impact kernel while accounting for uncertainty in the estimator, and derives asymptotic

optimality of strategies in terms of execution cost. In contrast, we suggest in-context learning, which combines offline and online learning in an efficient way, enhancing model flexibility while limiting the need for costly online learning. To the best of our knowledge, the only work that uses transformer models for trade execution is [KKSH24], which develops an adaptive dual-level reinforcement learning framework based on a combined transformer and Long-Short-Term Memory (LSTM) architecture in order to track the Volume-Weighted Average Price (VWAP). There has recently been also a lot of interest in the general learning of solution operators for ordinary and partial differential equations with varying network architectures. Among many others, we mention approaches based on Deep Operator Networks (DeepONet) in [LJP<sup>+</sup>21], graph kernels in [AAB<sup>+</sup>19], Fourier Neural Networks in [KLL<sup>+</sup>22], and structure-informed operator learning in [BDG24a, BDG24b].

The rest of the paper is organized as follows: Section 2 introduces the class of linear propagator models and the optimal liquidation problem, as well as a summary of the optimal solution. Our ICON-OCnet approach is described in Section 3. Numerical results are presented in Section 4. Conclusion and outlook are summarized in Section 5. For the sake of clarity and completeness, a short proof regarding the optimal execution strategies is collected in Appendix A.

## 2 Optimal liquidation with linear propagator models

We consider a classical optimal order execution problem with price impact within the general framework of linear propagator models. This class of models was originally developed by [BGPW04, BFL09] in discrete time and formulated by [Gat10] in continuous time; see also [BBG18, Chapter 13]. The associated optimal liquidation problem was explicitly solved only very recently in [AJN22], and we will also refer to [AJNV23, Section 3.2] for a simpler direct approach.

### 2.1 Model setup

We place ourselves in the setting of [AJN22]. Let  $T > 0$  denote a finite deterministic time horizon and fix a filtered probability space  $(\Omega, \mathcal{F}, \mathbb{F} := (\mathcal{F}_t)_{0 \leq t \leq T}, \mathbb{P})$  satisfying the usual conditions. We consider a trader with some initial inventory  $x \in \mathbb{R}$  in some risky asset (e.g., number of shares held in a stock) who wishes to liquidate her position by time  $T$  which represents, for instance, the end of the trading day. The trader's inventory, i.e., the number of shares held at any time  $t \in [0, T]$ , is modeled by the process  $X = (X_t)_{0 \leq t \leq T}$  with dynamics

$$X_t = x - \int_0^t u_s ds \quad (0 \leq t \leq T), \quad (1)$$

where  $u = (u_t)_{0 \leq t \leq T}$  denotes her selling rate, which is chosen from the set of admissible strategies

$$\mathcal{U} := \left\{ u : \mathbb{F}\text{-progressively measurable s.t. } \int_0^T \mathbb{E}[u_t^2] dt < \infty \right\}. \quad (2)$$

We assume that the trader's trading activity causes price impact in the sense that her trades are filled at the execution price

$$P_t = S_t - Y_t \quad (0 \leq t \leq T). \quad (3)$$

Here,  $S = (S_t)_{0 \leq t \leq T}$  denotes a square integrable special semimartingale and represents the unaffected price process, i.e., the price process that would have prevailed without the trader's trading, modeling price changes caused by other traders or the arrival of new information. In

contrast, the process  $Y = (Y_t)_{0 \leq t \leq T}$  models the trader's induced *transient* price impact that persists and decays over time. In the class of linear propagator models, this impact process is modeled as

$$Y_t = \int_0^t G(t-s)u_s\lambda ds \quad (0 \leq t \leq T) \quad (4)$$

with some price impact kernel  $G : [0, T] \rightarrow \mathbb{R}_+$  in  $L^2([0, T], \mathbb{R})$  (also called *propagator*) and constant push factor  $\lambda > 0$  (also referred to as *Kyle's lambda*). The types of parametric kernels  $G$  we are considering in (4) are as follows:

(I) *exponential kernels* as proposed by [OW13] of the form

$$G(t) = e^{-\beta t} \quad (0 \leq t \leq T) \quad (5)$$

with some impact decay parameter  $\beta > 0$ . In this case, note that  $Y$  in (4) is a Markovian process and satisfies the (random) linear ordinary differential equation (ODE)

$$Y_0 = 0, \quad \dot{Y}_t = -\beta Y_t + \lambda u_t \quad (0 \leq t \leq T). \quad (6)$$

(II) *power law kernels* as introduced by [BGPW04, Gat10] of the from

$$G(t) = \frac{1}{(\ell + t)^\gamma} \quad (0 \leq t \leq T) \quad (7)$$

for some shift parameter  $\ell \geq 0$  and decay elasticity  $\gamma > 0$ . We distinguish between (i) the non-singular case with  $\ell > 0$  and  $\gamma > 0$ , and (ii) the singular case with  $\ell = 0$  and  $\gamma \in (0, 0.5)$ . Observe that power law kernels induce non-Markovian dynamics for the impact process  $Y$  in (4).

Henceforth, we will also write the trader's execution price  $P$  in (3) as

$$P_t = S_t - (\mathbf{I}_\theta(u))_t \quad (8)$$

with transient price impact integral operator  $\mathbf{I}_\theta : L^2([0, T], \mathbb{R}) \rightarrow L^2([0, T], \mathbb{R})$ , which is induced by the kernel  $\lambda G$  with push factor  $\lambda$  and parametric  $G$  of either type (I) or (II), i.e.,

$$(\mathbf{I}_\theta(u))_t := \int_0^T G(t-s)1_{\{s \leq t\}}u_s\lambda ds = Y_t \quad (0 \leq t \leq T). \quad (9)$$

In particular, we interpret the operator  $\mathbf{I}_\theta$  as encoding the *price impact environment* in which the trader executes her trades, and we use the subscript  $\theta$  to emphasize the dependence on a certain price impact propagator model.

## 2.2 Optimization problem and optimal strategy

Following [AJN22], the trader's goal is to find an optimal order scheduling strategy  $u \in \mathcal{U}$  that maximizes her objective functional

$$J(u) := \mathbb{E} \left[ \int_0^T (S_t - (\mathbf{I}_\theta(u))_t)u_t dt - \varepsilon \int_0^T u_t^2 dt - \phi \int_0^T X_t^2 dt + X_T S_T - \varrho X_T^2 \right] \quad (10)$$

for some constants  $\varepsilon > 0$ ,  $\phi \geq 0$  and  $\varrho \geq 0$ . The first integral in (10) represents the trader's gains from her liquidation strategy  $u$ . The second integral with constant  $\varepsilon > 0$  describes in reduced form all additional *instantaneous costs*, which are not directly linked to persistent price impact but incurred, for instance, by the bid-ask spread; we also refer to the discussion

in [NWZ23]. The constants  $\phi \geq 0$  and  $\varrho \geq 0$  implement, respectively, a penalty on the running and terminal inventory as put forward in [CJP15, Chapter 6]. In particular, a large value for  $\varrho$  virtually enforces the desired liquidation constraint that  $X_T$  will be very close to zero. Finally, the term  $X_T S_T$  represents the final asset position's value in terms of the unaffected price. Observe that  $J(u) < \infty$  for any admissible  $u \in \mathcal{U}$ . To summarize, the aim of the trader is to solve the optimal stochastic control problem

$$J(u) \rightarrow \max_{u \in \mathcal{U}} . \quad (11)$$

The (semi-)explicit unique solution  $u^*$  of the optimal liquidation problem in (11) with propagators of type (I) and (II) was derived for the first time only very recently in [AJN22] by making a suitable ansatz on the value function. Here, we summarize the optimal strategy  $u^*$  by following the more direct approach from [AJNV23, Section 3.2] for the single-player case, leading to a slightly simpler representation. To this end, as argued in the proof of Proposition 2.1 below, we first note that the objective functional in (10) can be rewritten as

$$J(u) = \mathbb{E}[-\langle u, \mathbf{I}_\theta(u) \rangle - \langle u, \mathbf{C}(u) \rangle + \langle b, u \rangle + c]. \quad (12)$$

Here,  $\langle \cdot, \cdot \rangle$  denotes the usual inner product on  $L^2([0, T], \mathbb{R})$  and

$$\mathbf{C} := \varepsilon \text{id} + \tilde{\mathbf{C}} \quad (13)$$

represents another operator defined on  $L^2([0, T], \mathbb{R})$ , acting on the policies  $u \in \mathcal{U}$ , with identity operator  $(\text{id}(u))_t := u_t$  and integral operator  $\tilde{\mathbf{C}}$  induced by the kernel

$$\tilde{\mathbf{C}}(t-s) := 2\varrho 1_{\{s \leq t\}} + 2\phi(T-t)1_{\{s \leq t\}} \quad (0 \leq s, t \leq T) \quad (14)$$

in  $L^2([0, T], \mathbb{R})$ , i.e.,

$$(\mathbf{C}(u))_t = \varepsilon u_t + \int_0^T \tilde{\mathbf{C}}(t-s)u_s ds \quad (0 \leq t \leq T).$$

Moreover,  $b = (b_t)_{0 \leq t \leq T}$  is a square integrable stochastic process defined as

$$b_t := \mathbb{E}[S_t - S_T | \mathcal{F}_t] + 2(\phi(T-t) + \varrho)x \quad (0 \leq t \leq T) \quad (15)$$

and  $c$  is a random variable given by  $c := xS_T - \phi x^2 T - \varrho x^2$ . Observe that the objective in (12) conveniently decomposes into three parts: The first term  $\langle u, \mathbf{I}_\theta(u) \rangle$  is determined by the transient price impact operator  $\mathbf{I}_\theta$  in (9), i.e., the price impact environment. The second term  $\langle u, \mathbf{C}(u) \rangle$  is fully characterized by the hyperparameters  $\varepsilon, \phi, \varrho$ , which are chosen by the trader (controller) in (10). The third term  $\langle b, u \rangle$  reveals how the unaffected price process  $S$  in (3) ultimately affects the trader's performance functional. Specifically, note that  $b$  incorporates an (exogenous) *alpha signal*  $\alpha_t := \mathbb{E}[S_t - S_T | \mathcal{F}_t]$ ,  $t \in [0, T]$ , predicting the future returns of the unaffected stock price  $S$ . The signal is shifted by the trader's initial position  $x$ , scaled with the factor  $2(\phi(T-t) + \varrho)$ , which depends on the running and terminal inventory penalties  $\phi$  and  $\varrho$ . Lastly, the random variable  $c$  is just a by-product of the computations transforming (10) into (12) and does not influence the optimal strategy; cf. proof of Proposition 2.1 in Appendix A.

In order to state the optimal execution strategy, the following notation is needed: For a general kernel  $F : [0, T]^2 \rightarrow \mathbb{R}_+$  in  $L^2([0, T]^2, \mathbb{R})$ , we denote by  $\mathbf{F}$  the induced integral operator on  $L^2([0, T], \mathbb{R})$ , that is

$$(\mathbf{F}(g))_t := \int_0^T F(t, s)g_s ds, \quad g \in L^2([0, T], \mathbb{R}).$$

In addition, we define  $F_t(s, r) := F(s, r)1_{\{r \geq t\}}$  and write  $\mathbf{F}_t$  for the associated integral operator. We also denote by  $F^*(s, u) = F(u, s)$  the adjoint kernel of  $F$  and write  $\mathbf{F}^*$  for the corresponding adjoint integral operator. For more details, we refer to [AJN22] and [AJNV23], especially for the notion of the inverse of a kernel-induced integral operator in terms of a resolvent.

**Proposition 2.1.** *Assume that  $\varepsilon > 0$  and  $\varrho, \phi \geq 0$ . Then, the unique optimal strategy  $u^* \in \mathcal{U}$  in (11) with propagator kernels of type (I) and (II) is given by*

$$u_t^* = a_t + \int_0^t B(t, s) u_s^* ds \quad (0 \leq t \leq T), \quad (16)$$

where the stochastic process  $(a_t)_{0 \leq t \leq T}$  and the kernel  $B : [0, T]^2 \rightarrow \mathbb{R}$  are defined as

$$a_t := \frac{1}{2\varepsilon} (b_t - \langle 1_{\{t \leq \cdot\}} K(\cdot, t), \mathbf{D}_t^{-1} 1_{\{t \leq \cdot\}} \mathbb{E}[b | \mathcal{F}_t] \rangle), \quad (17)$$

$$B(t, s) := 1_{\{s \leq t\}} \frac{1}{2\varepsilon} (\langle 1_{\{t \leq \cdot\}} K(\cdot, t), \mathbf{D}_t^{-1} 1_{\{t \leq \cdot\}} K(\cdot, s) \rangle - K(t, s)), \quad (18)$$

$$\mathbf{D}_t := 2\varepsilon \text{id} + \mathbf{K}_t + \mathbf{K}_t^* \quad (19)$$

with  $K(t, s) := \tilde{C}(t - s) + \lambda G(t - s) 1_{\{s \leq t\}}$  for all  $0 \leq s, t \leq T$ .

The proof of Proposition 2.1 is a consequence of the results in [AJNV23] and provided in Appendix A for the sake of clarity and completeness. Observe that the solution to the integral equation in (16) can be stated as

$$u_t^* = ((\text{id} - \mathbf{B})^{-1}(a))_t \quad (0 \leq t \leq T) \quad (20)$$

with integral operator  $\mathbf{B}$  given by the kernel  $B$  defined in (18). Again, we refer to [AJN22, AJNV23] for more details, in particular for the existence of the inverse of the involved integral operators. Taking this even further, introducing the mapping  $b \mapsto a_t(b) := a_t$  with  $a_t$  as given in (17) for the process  $b$  in (15), we can introduce the *solution operator*  $\mathbf{S} : L^2([0, T]) \rightarrow L^2([0, T])$ , depending only on the operator  $\mathbf{I}_\theta + \mathbf{C}$  in (12) and acting on the optimization problem's (exogenous) input data  $b$ , defined as

$$(\mathbf{S}(b))_t := ((\text{id} - \mathbf{B})^{-1}(a(b)))_t \quad (0 \leq t \leq T). \quad (21)$$

Thus, we can rewrite the optimal solution  $u^*$  in (16) in a very compact form as

$$u_t^* = (\mathbf{S}(b))_t \quad (0 \leq t \leq T). \quad (22)$$

As described in [AJN22, Section 5], the optimal liquidation strategy can be computed numerically very efficiently by a discretization scheme applied to the integral equation in (16), where the representation in (20) boils down to a matrix inversion and matrix vector multiplication. We utilize the method presented therein to compute the ground truth optimal benchmark strategies  $u^*$  for *known* price impact operators  $\mathbf{I}_\theta(\cdot)$  in our numerical illustrations in Section 4. Generally speaking, our goal in the remainder of this paper is to develop a methodology which numerically evaluates the solution operator  $\mathbf{S}$  in (22) when the price impact operator  $\mathbf{I}_\theta(\cdot)$  in (9) is *unknown*; see Section 3 below.

**Remark 2.2.** *The representation of the optimal strategy  $u^*$  in (16) is equivalent to the expression derived in [AJN22, Proposition 4.5] but a little bit simpler; cf. equations (4.15) and (4.16) therein.*

**Remark 2.3.** Observe that the only source of randomness in the optimal stochastic control problem in (12) is the alpha signal  $\alpha_t = \mathbb{E}[S_t - S_T | \mathcal{F}_t]$  in the process  $b$  in (15), entering the stochastic input process  $a$  in (17). In particular, if the unaffected price process  $S$  in (3) is a martingale, the optimization problem of maximizing (12) or equivalently (10) over  $\mathcal{U}$  reduces to a deterministic control problem and the optimal execution strategy in (20) is a deterministic function in time  $t \in [0, T]$ .

### 2.3 Model parameters

We adopt the parameter configuration used in [NWZ23, Section 3]. The time unit is trading days and denoted by  $[T]$ . We set  $T = 1$  so that the strategy trades during one trading day over the interval  $[0, 1]$  (i.e., 6.5 hours during Nasdaq's opening hours). All trading quantities are expressed as a percentage of the *Average Daily Volume* (ADV%) and we denote by  $[V]$  the volume unit. For instance, a sell order with initial size  $x = 0.1 [V]$  represents a sell order of size 10% ADV. Accordingly, the trading rate  $u$  in (1) is measured in  $[V][T]^{-1}$ . We focus on a range of  $[0.01, 0.20]$  for the initial inventory  $x$ .

The natural (absolute) unit of  $Y$  (and the unaffected price process  $S$ ) in (3) is USD  $[\$]$ . Ultimately, however, it is more common to think of the price impact  $Y$  (and its associated costs) in terms of basis points (bps) relative to some initial benchmark price (e.g., the prevailing decision price  $P_0 = S_0$  at the beginning of the trading period). The performance functional in (10) is then also standardized accordingly to represent total implementation shortfall costs in basis points. Therefore, in the units of the parameters below, we treat  $Y$  as unitless (i.e., standardized). For the kernel parameters in (I) and (II), and the push factor  $\lambda$ , we focus on the following ranges:

- (i) The impact decay  $\beta$  in (6) has unit  $[T]^{-1}$  and describes the speed at which impact reverts to zero. The corresponding half-life is given by  $\log(2)/\beta$ . We let  $\beta$  vary in the interval  $[0.462, 9.011]$ , which roughly corresponds to half-lives ranging from 30 minutes to 1.5 days.
- (ii) The push factor  $\lambda$  in (4) has unit  $[V]^{-1}$  with values in  $[0.1, 0.5]$ .
- (iii) The power law kernel in (7) captures multiple timescales of decay in a parsimonious way. In the non-singular case, we set  $\ell = 1$  and let  $\gamma$  vary in  $[0.3, 1.5]$ . For the singular case  $\ell = 0$ , we restrict  $\gamma$  to  $[0.35, 0.45]$ .

## 3 Price impact operator learning and neural network solver

In this section, we describe the in-context price impact learning task and downstream optimization algorithm used to find the optimal liquidation strategy in (11) with *unknown* price impact operator  $\mathbf{I}_\theta$ . An illustration of the method, which we coin ICON-OCnet, is shown in Figure 1. It consists of two steps summarized as follows:

1. Train ICON offline in a data-driven way on a range of propagator models  $\theta$  with different kernels and parameters. Then, use the pre-trained ICON model in a few-shot online learning manner to infer the operator  $\mathbf{I}_{\tilde{\theta}}$  mapping  $u$  onto  $Y$  in (9) based on only a few examples of  $(u, Y)$  pairs, stemming from a specific model  $\tilde{\theta}$ , possibly not seen during offline training.
2. Train a neural network policy (OCnet) via a policy gradient method to approximate the optimal execution strategy in (11) based on the ICON surrogate operator  $\hat{\mathbf{I}}_{\tilde{\theta}}$  obtained in

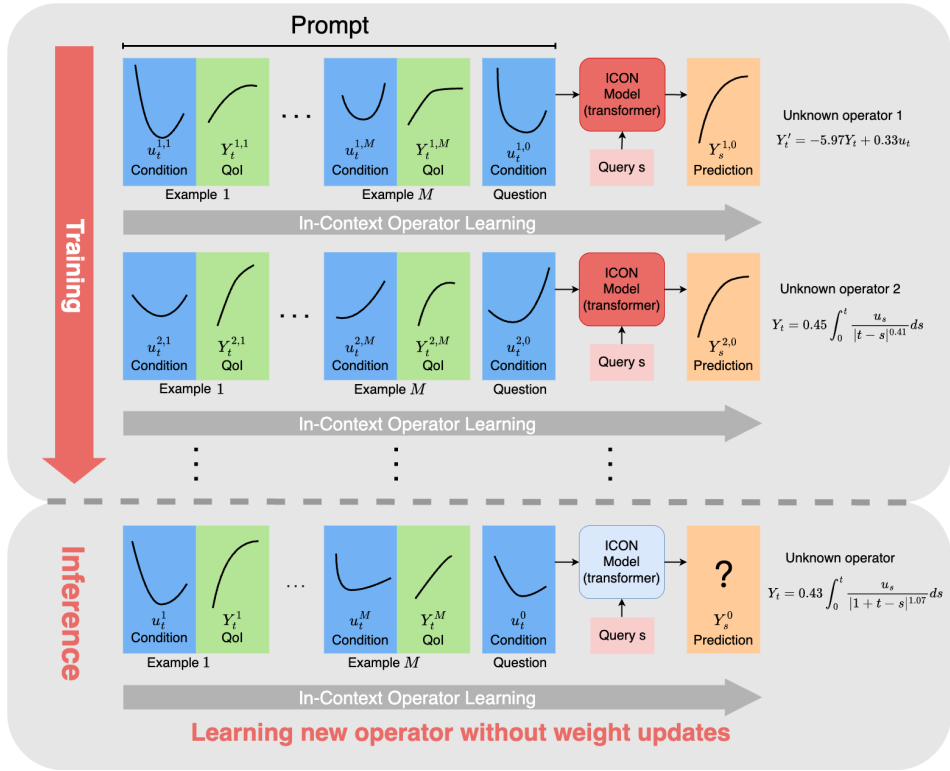
step 1. In particular, the performance measure for training OCnet is a discretization of the objective functional in (10) with  $Y_t = (\mathbf{I}_{\tilde{\theta}}(u))_t$  replaced by the in-context prediction  $(\hat{\mathbf{I}}_{\tilde{\theta}}(u))_t$  of ICON.

### 3.1 ICON training and few-shot learning

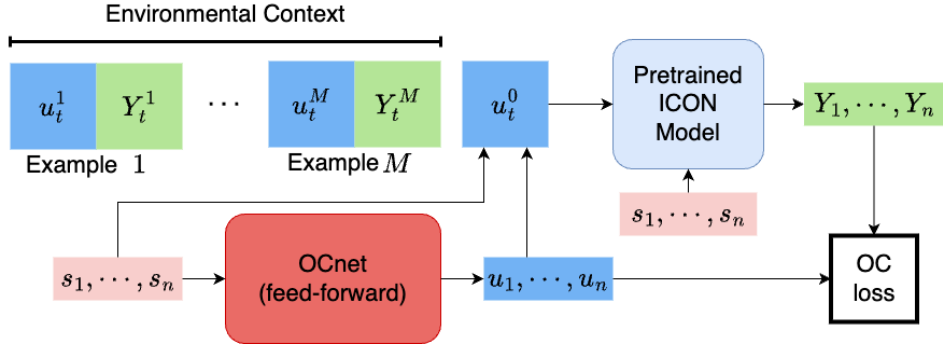
Concerning step 1, inspired by [YLMO23], we use In-Context Operator Networks (ICON), a novel transformer-based neural network architecture designed to learn the operator  $\mathbf{I}_{\theta} : L^2([0, T], \mathbb{R}) \rightarrow L^2([0, T], \mathbb{R})$  defined in (9) that maps the trading rate process  $u$  to the price impact process  $Y = \mathbf{I}_{\theta}(u)$ . The network is pre-trained in an offline learning step, and can then, in a second online learning step, detect the price impact operator from a few provided examples. Unlike traditional neural network methods, which require re-training or fine-tuning for each new problem, the so-called few-shot learning or prompting technique used here only requires a few sample trades and their respective price impact in order to recognize the underlying relationship between  $u$  and  $Y$ . In particular, it can deal with new unseen price impact models without actually retraining the network weights. This allows the network to handle a wide range of price impact models by leveraging commonalities shared between different models. From a practical perspective, this methodology has several advantages. First, the true relationship  $u \mapsto Y$  is typically unknown. Even after a decision on a specific model has been made, there might be uncertainty about the parameters of the model. Moreover, the model parameters might not be constant over time. With the in-context few-shot learning approach, a trading desk tasked with liquidating a large position can, in principle, base its search for an optimal execution strategy in a data-driven way on *experience* from recent trades of the same asset. In this way, the network architecture automatically detects, from a universe of possible price impact models, a model that best fits the most recent *observed* price impact as provided by the few examples or test trades as context.

Using a transformer architecture also offers multiple benefits for our few-shot prompting task in the context of optimal liquidation with propagator models. First, its attention mechanism allows the neural network to efficiently process inputs of varying lengths, making it well suited for handling different types of examples (data prompts) and key-value pairs (i.e., time instances  $s_j$  and observations  $(u_{s_j}, Y_{s_j})$ ) without necessitating structural changes. From a practical point of view, this flexibility is very helpful in learning the true price impact operator. Indeed, the test trades and the corresponding observed price impact that are used as examples are usually not uniform in length and discretized at different time steps. Second, transformers are invariant to the order of the input data, ensuring that the order of the examples does not affect the few-shot inference. Moreover, and most importantly for our purpose, the multi-head attention mechanism of the transformer is very well suited for *sequential data* and enables it to capture the relationships between different parts of the input. This facilitates the learning of the price impact by focusing on the most relevant aspects of the examples. As a consequence, transformers can deal with complex interdependencies, making them a very natural choice for the non-Markovian propagator models, which relate price moves intertemporally to current and past trades. Lastly, transformers also support parallel processing, rendering it computationally efficient to generate predictions across multiple query points simultaneously, which is vital for fast inference in few-shot settings. We also refer to the discussion in [YLMO23].

The in-context learning procedure and few-shot prompting inference of the ICON model are illustrated in Figure 1 (a). Each row above the dashed line represents one data point that is used in training. The data in row  $i$  is produced by the same price impact model  $\theta_i$  and consists of  $M$  condition and quantity of interest (QoI) pairs  $(u^{i,1}, Y^{i,1}), \dots, (u^{i,M}, Y^{i,M})$



(a) Step 1: ICON training



(b) Step 2: OCnet training

Figure 1: Illustration of the ICON-OCnet structure. In both steps, the red rounded rectangle represents the training of a neural network, while the blue rounded rectangle indicates a pre-trained neural network with frozen parameters.

serving as the context, followed by the actual question condition  $u^{i,0}$ , a query  $(s_1, \dots, s_k)$ , and the corresponding output  $(Y_{s_1}^{i,0}, \dots, Y_{s_k}^{i,0})$ . The query provides ICON with the grid information (discretization) on which  $Y$  is evaluated. Note that the discretization for the question condition can be different from the discretization of the example pairs, which themselves can differ across the examples. Based on this data, ICON is trained in an offline manner. We use masking to ensure that  $Y$  is non-anticipative with respect to  $u$  and the provided examples during the learning process. Next, at the inference stage illustrated below the dashed line in Figure 1 (a), the trained ICON network is presented with  $M$  new examples (data prompts) stemming from a (possibly unseen) model  $\tilde{\theta}$ . Based on these examples, the pre-trained ICON network infers the underlying operator  $\mathbf{I}_{\tilde{\theta}}$  and provides the output prediction for an arbitrary question condition  $u^0$  at an arbitrary query  $(s_1, \dots, s_l)$ . In other words, it predicts the price impact  $Y = \mathbf{I}_{\tilde{\theta}}(u^0)$  of a strategy  $u^0$  on the grid  $(s_1, \dots, s_l)$  for a *possibly unknown model*  $\tilde{\theta}$  that generated the example data as context. Moreover, predictions of the price impact  $\mathbf{I}_{\tilde{\theta}}(u)$  for any strategy  $u \in \mathcal{U}$  on a varying grid can then be obtained by providing as context the same  $M$  examples from the underlying model  $\tilde{\theta}$  in every inference step. In this way, we obtain an ICON *surrogate operator*  $\hat{\mathbf{I}}_{\tilde{\theta}}$  for the true operator  $\mathbf{I}_{\tilde{\theta}}$  that we can feed into an optimization algorithm to compute the corresponding optimal order execution strategy in (11). The subscript  $\tilde{\theta}$  in the notation for the surrogate operator  $\hat{\mathbf{I}}_{\tilde{\theta}}$  emphasizes that the provided context (examples) originate from the same model  $\tilde{\theta}$ .

Our ICON neural network architecture corresponds to the one used in [YLMO23]. More details on the training are provided in Sections 4.1 and 4.2.

### 3.2 Neural network solver with ICON surrogate

We now explain the general methodology for step 2, that is, the OCnet training for the optimal liquidation strategy using ICON as a proxy for the price impact operator. More precisely, (i) as described above, based on only  $M$  example trades provided as context, ICON infers a model (here represented by  $\theta$ ) and we obtain the ICON surrogate operator  $\hat{\mathbf{I}}_\theta$ , which approximates the true price impact operator  $\mathbf{I}_\theta$  in (9); (ii) we feed  $\hat{\mathbf{I}}_\theta$  into the optimization problem in (11) and train a neural network policy (OCnet) to approximate the optimal execution strategy in the presence of the current market environment detected by ICON.

Put differently, the optimization problem becomes

$$\max_{u \in \mathcal{U}} \mathbb{E} \left[ \int_0^T \left( (S_t - (\hat{\mathbf{I}}_\theta(u))_t) u_t - \varepsilon u_t^2 - \phi X_t^2 \right) dt + X_T S_T - \varrho X_T^2 \right], \quad (23)$$

where the in-context transformer network predicts the transient price impact

$$Y_t \approx \hat{\mathbf{I}}_\theta(t, (u_s)_{0 \leq s \leq t}; (u_s^1, Y_s^1)_{0 \leq s \leq t}, \dots, (u_s^M, Y_s^M)_{0 \leq s \leq t}) \quad (0 \leq t \leq T) \quad (24)$$

incurred by a strategy  $u \in \mathcal{U}$ . With a slight abuse of notation in (24), we make explicit the effect of masking, the path dependence of  $Y_t$  on all past trades  $(u_s)_{0 \leq s \leq t}$ , as well as the dependence on the  $M$  fixed examples up to time  $t$  provided as context.

Next, we assume that trading takes places on an equidistant time grid  $t_i = i\Delta t$ ,  $i = 0, \dots, N$ , with  $\Delta t = T/N$ , generate  $L$  samples  $(S_{t_i}^{(l)})_{i=0, \dots, N}$ ,  $1 \leq l \leq L$ , of the unaffected price process  $(S_t)_{0 \leq t \leq T}$  in (3), and approximate (23) via

$$\frac{1}{L} \sum_{l=1}^L \left\{ \sum_{i=0}^{N-1} \left( (S_{t_i}^{(l)} - \hat{\mathbf{I}}_\theta(t_i, u_{t_0}, \dots, u_{t_i})) u_{t_i} - \varepsilon u_{t_i}^2 - \phi X_{t_i}^2 \right) \Delta t + X_{t_N} S_{t_N}^{(l)} - \varrho X_{t_N}^2 \right\} \rightarrow \max_{u \in \mathcal{N}} \quad (25)$$

with  $X_{t_i} = x - \sum_{j=0}^{i-1} u_{t_j} \Delta t$ . Here,  $\mathcal{N}$  denotes the set of all feed-forward neural network policies of the form  $\text{NN}_\vartheta(t, a)$  with  $\text{NN}_\vartheta : [0, T] \times \mathbb{R} \rightarrow \mathbb{R}$  and some fixed architecture parameterized by  $\vartheta \in \mathbb{R}^m$  for some  $m \in \mathbb{N}$ . Specifically, the (semi-)explicit result of the optimal solution with *known* price impact operator  $\mathbf{I}_\theta$  summarized above in (22) motivates in (25) to search for neural network feedback policies  $\text{NN}_\vartheta \in \mathcal{N}$  with input  $(t_i, \alpha_{t_i})$ , i.e.,  $u_{t_i} = \text{NN}_\vartheta(t_i, \alpha_{t_i})$  and alpha signal  $\alpha_t = \mathbb{E}[S_t - S_T | \mathcal{F}_t]$ . The optimal strategy can then be readily computed by employing a policy gradient method; that is, adopting the approach in [HE16], running a stochastic gradient descent-type algorithm (scheduled AdamW) on the discrete objective functional in (25) with respect to the neural network parameters  $\vartheta$ . We refer to the obtained optimal execution strategy as the OCnet policy. More details on the OCnet training are provided in Section 4.3.

## 4 Numerical results

In this section, we describe our numerical experiments and the results obtained. In summary, we illustrate the following:

1. The trained ICON model is capable of accurately inferring the underlying price impact model from only  $M = 5$  examples provided as context, even for propagator models not present in the training data.
2. Using ICON as a surrogate operator in the optimal execution problem (ICON-OCnet) correctly retrieves the ground truth optimal execution strategies  $u^*$  in (20) for various propagator models generating the five examples as context.

Throughout our numerical study, we set  $T = 1$  and perform all training steps for ICON and OCnet, including the in-context examples and queries for the predictions, on a fixed equidistant time grid with  $N = 100$  steps. Note that this is merely for simplicity and not a requirement. In addition, the hyperparameters in the optimal control problem in (25) are set as follows: we fix the instantaneous cost parameter  $\varepsilon$  at 0.5 and set  $\phi = 0$  for the penalty on the running inventory in accordance with the implementation of the ground truth optimal strategies  $u^*$  in (20) provided by [AJN22], which we use as our benchmark. We also let the penalization on the terminal inventory  $\varrho$  be equal to 10 to enforce the liquidation constraint  $X_T \approx 0$ .

Moreover, to get a clear picture of the performance of our ICON-OCnet methodology, we focus as in [NSZ23, Section 3] on the deterministic base case as a testbed and “neutralize” the effects of an exogenous alpha signal by assuming that the unaffected price process  $S$  in (3) is a martingale. Note that this implies  $\alpha \equiv 0$ . Hence, without loss of generality, it suffices to optimize in (25) with  $S \equiv 0$  over neural network policies that are functions in time only; cf. also Remark 2.3. In particular, we know from the results in [AJN22] that in this case the optimal selling rates  $u^*$  in (20) to liquidate an initial positive inventory  $x > 0$  are strictly positive, smooth U-shaped deterministic functions in time with varying curvature depending on the propagator kernel  $G$  and the push factor  $\lambda$ . We refer to [AJN22, Section 5.2] for more details.

### 4.1 Data generation

For the offline training step of ICON (recall Figure 1 (a)), we generate three different synthetic datasets of selling rates and price impact pairs  $(u, Y)$  corresponding to the three different kernels in (5) and (7): exponential, non-singular power law, singular power law. Here, we take the exponential kernel in (5) as an example to explain our training methodology. First,

we randomly sample 80,000 pairs of hyperparameters  $\theta = (\lambda, \beta)$  for the push factor  $\lambda \sim U([0.1, 0.5])$  and the impact decay  $\beta \sim U([0.462, 9.011])$ ; cf. also Section 2.3. Next, for each  $\theta$ , we generate 10 strictly positive selling rates  $u = \tilde{u} + 0.1$ , where  $\tilde{u}$  is sampled from a smooth Gaussian process on  $[0, 1]$  with kernel  $0.05^2 \exp(-2t^2)$ . Recall from Section 2.3 that the selling rate is measured in  $[V][T]^{-1}$  with ADV as volume unit. We then compute for each  $u$  the corresponding price impact  $Y = \mathbf{I}_\theta(u)$  using a discretized version of (9). The other two datasets for the power law kernels in (7) are generated similarly, with hyperparameters  $\lambda \sim U([0.1, 0.5])$ ,  $\gamma \sim U([0.3, 1.5])$  and  $\ell = 1$  for the non-singular kernel; and  $\lambda \sim U([0.1, 0.5])$ ,  $\gamma \sim U([0.35, 0.45])$  for the singular kernel with  $\ell = 0$ . An illustration of 10 sample trajectories used in training is shown in Figure 2.

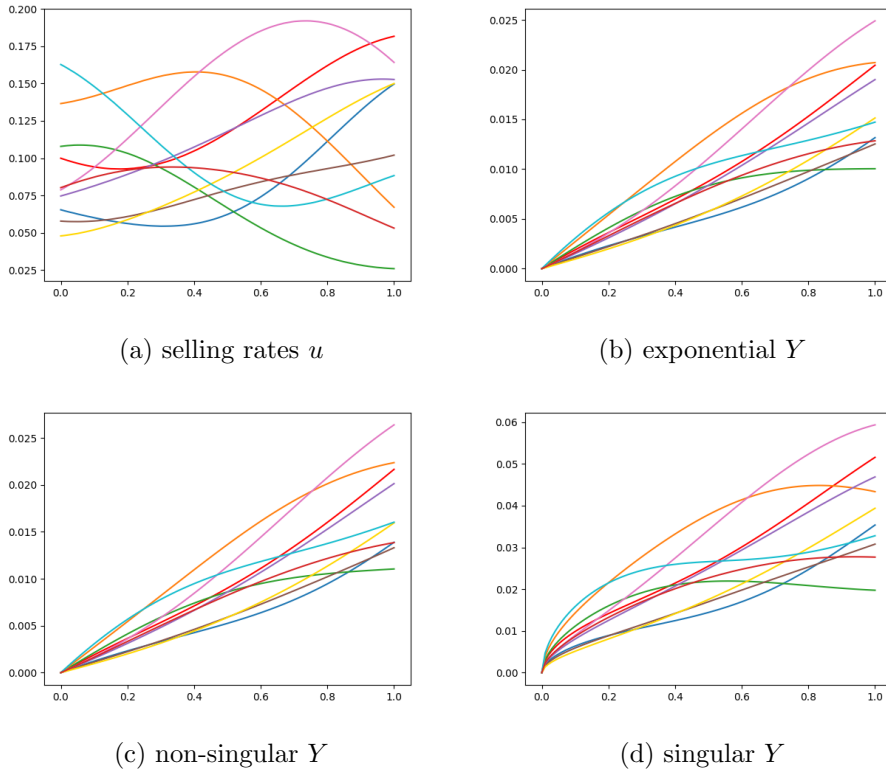


Figure 2: Illustration of 10 training trajectories (selling rates  $u$  and corresponding price impact  $Y$ ) for the three different kernels with parameters  $\lambda = 0.2$ ,  $\beta = 0.5$ ,  $\gamma = 0.45$ .

During each iteration in the training process of ICON, a mini-batch of size 8 of hyperparameters  $\theta_i$ ,  $i = 1, \dots, 8$ , is randomly selected from the 80,000 generated data points. Then, for each such  $\theta_i$  with associated 10 generated sample pairs  $((u^{i,1}, Y^{i,1}), \dots, (u^{i,10}, Y^{i,10}))$  as described above, we randomly select one pair as the input-output pair (i.e., question condition  $u^{i,0}$  and labeled output  $Y^{i,0}$  as illustrated in Figure 1 (a)); and from the remaining 9 pairs we randomly select  $M = 5$  to serve as examples in the context. A stochastic gradient descent step (using scheduled AdamW) on the training loss function (i.e., update on the ICON's parameters) is then performed with this mini-batch of 8 data points.

## 4.2 ICON performance

In this section, we evaluate the performance of ICON training described in Section 3.1. In total, four different ICON models are trained: (i) three models, each trained on a separate propagator model dataset `ode`, `ker`, `sker` generated from the three different propagator kernels

exponential (`ode`), non-singular power law (`ker`), singular power law (`sker`) as described above in Section 4.1; (ii) a fourth model trained on a mixed dataset `all3` that combines the previous three datasets. To ensure a fair comparison, the number of training samples is 80,000 in all four datasets (i.e., in `all3` only 1/3 of each dataset `ode`, `ker`, `sker` of size 80,000 is used). We use the same ICON neural network architecture as in [YLMO23]<sup>1</sup> and train all four ICON models for 100,000 iterations.<sup>2</sup> The resulting  $\ell^2$  relative error is plotted in Figure 3 against the number of iterations.

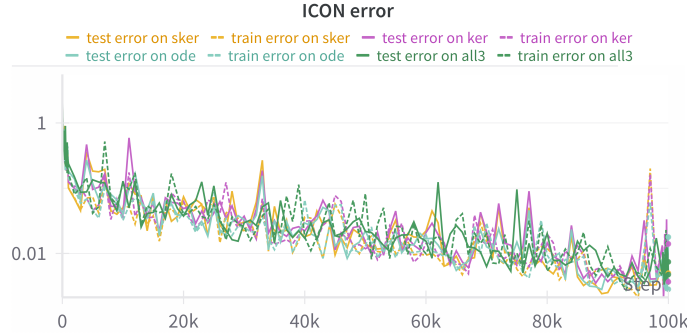


Figure 3: ICON error (on the training set and a separate test set) versus training iterations with 100,000 training steps in total.

After training, we assess the relative  $\ell^2$  errors of all four ICON model predictions  $\hat{\mathbf{I}}_\theta(u)$  with respect to the exact output  $Y = \mathbf{I}_\theta(u)$  of the provided question condition  $u$ , for various in-context examples from propagator models  $\theta$  from out-of-sample test datasets. In particular, we examine the out-of-distribution performance (i.e., transfer learning) of the first three ICON models (trained separately on `ode`, `ker`, `sker`, respectively) on in-context examples from a propagator kernel type not seen during the training phase. The test datasets, denoted by `ode_t`, `ker_t`, `sker_t`, are generated using the exact same methodology as for the training data described in Section 4.1. The results are summarized in Table 1. Each column represents a trained ICON model and each row corresponds to a specific test dataset for the in-context examples. For each combination, we calculate mean and standard deviation of the prediction error for a sample of size 576. The in-distribution errors (bold values in the diagonal of the first three columns) are very small for each ICON model, illustrating that the trained ICON models are capable of accurately inferring the underlying propagator model from the  $M = 5$  in-context examples. Moreover, also the out-of-distribution errors for the transfer learning are quite small (off-diagonal entries of the first three columns). Hence, the ICON prediction based on few-shot learning from the prompted examples generalizes fairly well to unseen propagator kernel types. We also observe that the ICON model trained on the mixed dataset `all3` performs very well across all three in-context example training sets.

Next, we present in Figure 4 heatmaps which shed some light on the dependence of the ICON models' in-distribution prediction errors with respect to the underlying price impact model parameters generating the in-context examples. More precisely, the two axes represent the hyperparameters  $\theta$  for each kernel type (I) and (II) (split in 6 intervals), with the color of each box indicating the mean error of the ICON prediction for 16 randomly selected hyperparameters within the box's range which are used for generating the in-context example pairs and the exact output label  $\mathbf{I}_\theta(u)$  of the question condition  $u$  (again, everything is generated using the same method as described in Section 4.1). Note that the error remains invariant

<sup>1</sup>Transformer with 6 layers, 8 heads, head dimension 256, model dimension 256, widening factor 4.

<sup>2</sup>Training is performed on a single NVIDIA GeForce RTX 4090 GPU and takes about 3.5 hours.

	ode	ker	sker	all3
ode_t	<b>0.0053 ± 0.0045</b>	0.1075 ± 0.1266	0.1635 ± 0.2369	0.0060 ± 0.0044
ker_t	0.0072 ± 0.0057	<b>0.0045 ± 0.0024</b>	0.0345 ± 0.0309	0.0063 ± 0.0048
sker_t	0.0423 ± 0.0191	0.0392 ± 0.0241	<b>0.0052 ± 0.0036</b>	0.0057 ± 0.0036

Table 1: ICON error table of relative  $\ell^2$  prediction errors. Each column corresponds to one of the four ICON models trained on a specific dataset. The rows represent the different test datasets for the 5 in-context examples.

with respect to the push factor  $\lambda$  due to the scaling-invariant property of our ICON architecture. With regards to the impact decay  $\beta$  in the exponential kernel, the error becomes smaller with faster decay (Figure 4, (a) and (b)). For the power law kernel, the influence of  $\gamma$  shows a slightly less coherent pattern across the different ICON models `ker`, `sker`, `all3` (Figure 4, (c)–(f)); perhaps not surprisingly due to the more subtle nature of a power law decay. Overall, however, the errors are very small.

Finally, we evaluate how well ICON generalizes to *unseen* selling rates  $u$  as question conditions, that is, strategies which are not directly generated from the Gaussian process as in the synthetic training datasets. This is a first sanity check of ICON’s effectiveness as a surrogate operator in the downstream optimal execution problem in (25), i.e., our ICON-OCnet approach. To this end, we generate five synthetic examples as context from a specific propagator model  $\theta$  using the same method as described in Section 4.1. However, for the in-context prediction task, we use as question condition the actual (out-of-distribution) ground truth optimal execution strategy  $u^*$  of model  $\theta$  which is computed via the implementation provided by [AJN22]. We then compute the corresponding optimal price impact process  $Y^* = \mathbf{I}_\theta(u^*)$  to obtain the exact output label, and compare it to the prediction of the ICON surrogate operator  $\hat{\mathbf{I}}_\theta(u^*)$  acting on  $u^*$ . The relative  $\ell^2$  error under this setup is computed and visualized as heatmaps with varying hyperparameters in Figure 5, similar to the ones in Figure 4. This time, the error increases slightly, but still remains fairly small across the different ICON models and test datasets providing the context. We also observe that here, different compared to Figure 4, the errors depend on the push factor  $\lambda$ , simply because variations in  $\lambda$  alter the question condition  $u^*$ .

To further elaborate on the previous analysis, we illustrate in Figure 6 five pairs of in-context examples  $((u^{i,1}, Y^{i,1}), \dots, (u^{i,5}, Y^{i,5}))$  for  $i = 1, 2, 3$  different propagator models with randomly sampled hyperparameters  $\theta_i$ , generated as described in Section 4.1; the question condition  $u^{i,*}$  (i.e., the optimal execution strategy for model  $\theta_i$ ); and the prediction curves  $\hat{\mathbf{I}}_{\theta_i}(u^{i,*})$  compared to the ground truth price impact  $\mathbf{I}_{\theta_i}(u^{i,*})$ . More precisely, each subfigure in Figure 6 corresponds to a specific model  $\theta_i$  (exponential kernel in (a), non-singular power law kernel in (b), singular power law kernel in (c)). The top panel of each subfigure displays the in-context example conditions  $u^{i,1}, \dots, u^{i,5}$  in colored solid lines, as well as the question condition  $u^{i,*}$  in black dotted lines. The middle panel shows the corresponding in-context example quantities of interest  $Y^{i,1} = \mathbf{I}_{\theta_i}(u^{i,1}), \dots, Y^{i,5} = \mathbf{I}_{\theta_i}(u^{i,5})$ . The bottom panel compares the in-context prediction  $\hat{\mathbf{I}}_{\theta_i}(u^{i,*})$  (red solid line) of the ICON model (trained on the dataset `ode` in (a), `ker` in (b), `sker` in (c), respectively) with the ground truth  $\mathbf{I}_{\theta_i}(u^{i,*})$  (black dotted line). Note that the optimal execution strategies  $u^{i,*}$  are almost flat for the three different propagator kernels with (randomly picked) hyperparameters  $\theta_i$ . Remarkably, we observe that the three ICON surrogate operators are indeed capable of accurately predicting the corresponding price impact incurred by the selling rates  $u^{1,*}, u^{2,*}, u^{3,*}$ , which gradually build up at different speeds and magnitudes, depending on the different propagator kernels and their hyperparameters  $\theta_1 = (\beta_1, \lambda_1)$  (for the exponential kernel),  $\theta_2 = (\gamma_1, \lambda_2)$  (for the non-

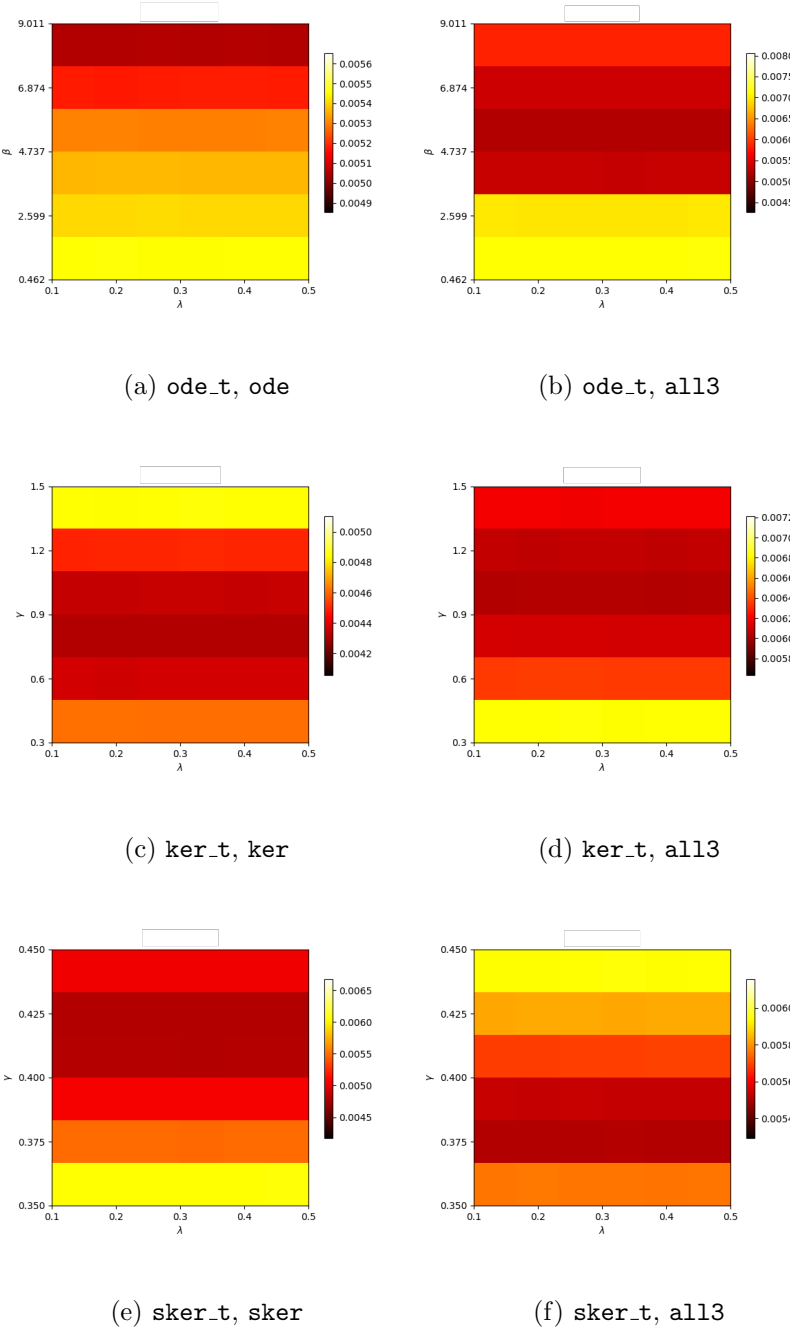


Figure 4: Heatmaps for ICON in-distribution errors for different types of in-context examples (first label) and ICON models trained on a specific dataset (second label). The value of each box represents the mean error over 16 random samples of sets of hyperparameters  $\theta$  from the corresponding ranges, generating the five in-context examples ( $x$ -axis represents values for  $\lambda$ ,  $y$ -axis represents values for  $\beta$  and  $\gamma$ , respectively).

singular power law kernel) and  $\theta_3 = (\gamma_2, \lambda_3)$  (for the singular power law kernel), all of which are correctly inferred by the ICON models from the five prompted in-context examples.

### 4.3 ICON-OCnet performance

We now illustrate the performance of our ICON-OCnet method described in Section 3.2. Specifically, using a pretrained ICON model as described above (trained on `ode`, `ker`, `sker`, `a113`, respectively, and prompted with 5 in-context examples from a specific propagator model  $\theta$ ) as a surrogate operator  $\hat{\mathbf{I}}_\theta$  in the optimal execution problem, we perform a policy gradient method directly on the objective function in (25), and train a simple feed-forward neural network<sup>3</sup> with 60,000 iterations for the optimal order execution task. The initial inventory  $x$  expressed in ADV is sampled from a uniform distribution  $U([0.01, 0.2])$ . We compare the obtained OCnet policy  $\hat{u}$  (with corresponding inventory  $\hat{X}$  and price impact process  $\hat{Y}$ ) to the actual ground truth optimal execution strategy  $u^*$  in (20) (with state processes  $X^*, Y^*$ ) of the propagator model  $\theta$  generating the in-context examples, which is computed via the implementation provided by [AJN22].

The relative  $\ell^2$  errors of selling rate, inventory, and price impact process (compared with the ground truth) versus the number of training steps are illustrated in Figure 7. We observe convergence of the policy gradient method after 60,000 iterations. In fact, the errors already drop to an acceptable level after 20,000 steps.

Table 2 summarizes the relative error of the objective function value in (25) of the trained OCnet policy  $\hat{u}, \hat{Y}, \hat{X}$  with respect to the actual value of the objective function of the ground truth optimal policy  $u^*, Y^*, X^*$ . The three different ICON models (columns) are trained on a single correct dataset (i.e., the prompted in-context examples in the optimization problem are originating from the same propagator kernel type on which the ICON model was pre-trained). We observe that the error values are impressively small. This confirms the effectiveness of our proposed ICON-OCnet approach in finding the *optimal execution strategy* via few-shot in-context learning with ICON. Sample trajectories of the obtained OCnet selling rate  $\hat{u}$  and corresponding price impact  $\hat{Y}$  compared to the ground truth optimal execution strategy  $u^*$  and impact process  $Y^*$  for different propagator kernels (with randomly chosen hyperparameters  $\theta$  and initial inventory  $x$ ) are shown in Figure 8.

	<code>ode</code>	<code>ker</code>	<code>sker</code>
ICON-OCnet	$5.80 \times 10^{-8}$	$6.91 \times 10^{-7}$	$4.55 \times 10^{-7}$

Table 2: Relative error of the optimal control objective function value for ICON models trained on a single correct dataset (rows). The values are averaged over 16 sets of randomly selected hyperparameters  $\theta$  and initial inventories  $x$ .

Lastly, we illustrate the influence of the hyperparameters on the error of ICON-OCnet in the heatmaps in Figures 9 and 10. Similarly to the heatmaps in Section 4.2, we split the range of each hyperparameter into 6 intervals, and then randomly sample in each box 16 sets of hyperparameters (and initial inventories  $x$ ), for which we train an OCnet policy with the pretrained ICON model (trained on a single dataset in Figure 9 or on the mixed dataset in Figure 10), prompted with in-distribution examples as context, and compute the relative  $\ell^2$  error of  $\hat{u}, \hat{X}, \hat{Y}$  with respect to the corresponding ground truths  $u^*, X^*, Y^*$ . Overall, the errors are fairly small. As expected, the errors increase slightly when ICON is trained on the mixed dataset `a113`.

<sup>3</sup>The OCnet neural network structure consists of 2 hidden layers, 128 nodes in each layer, and GELU activation function.

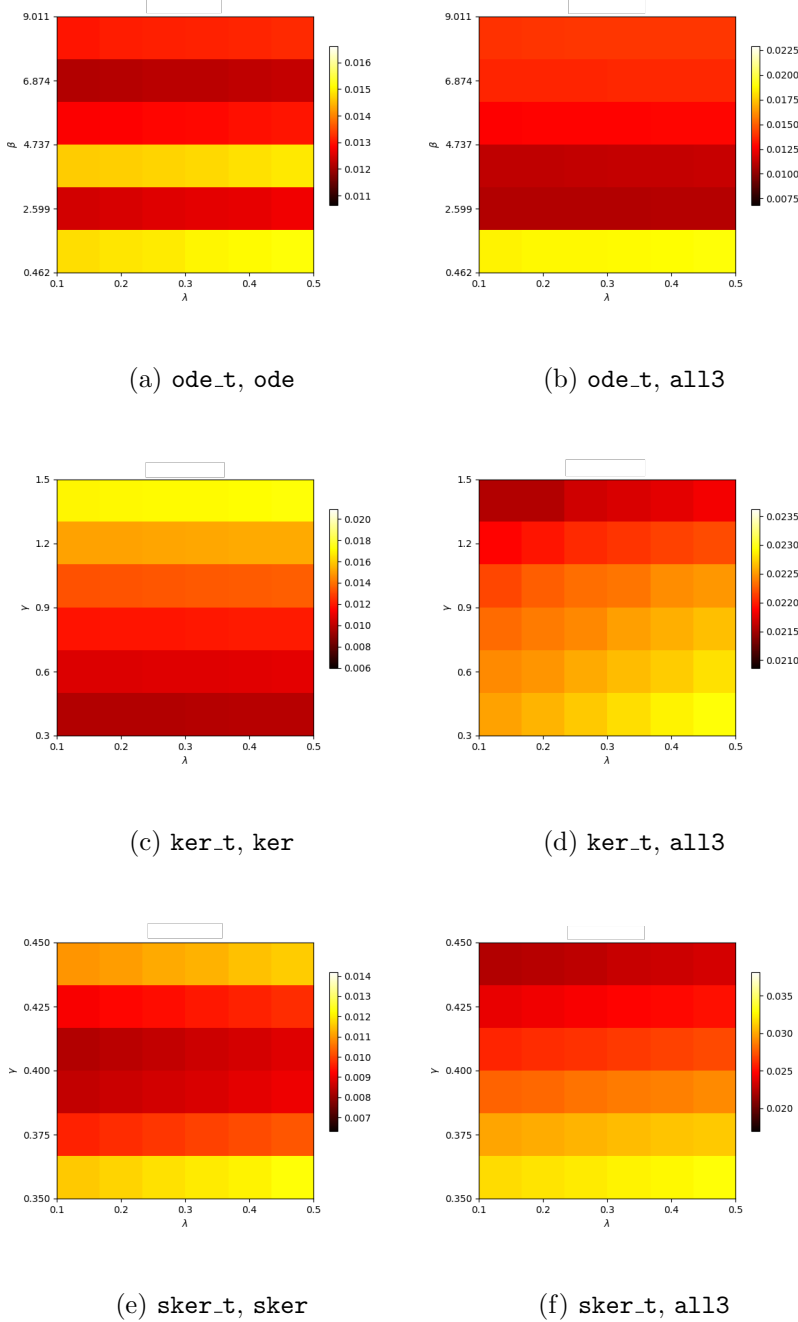
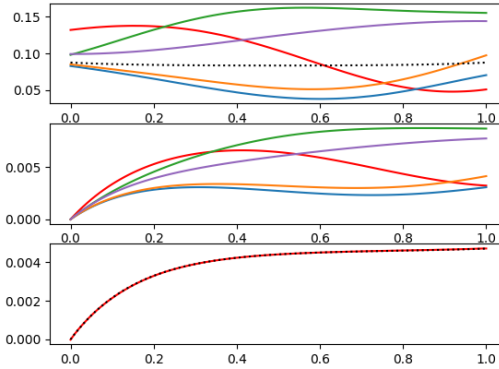
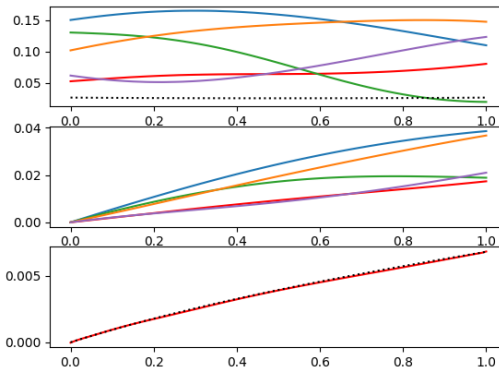


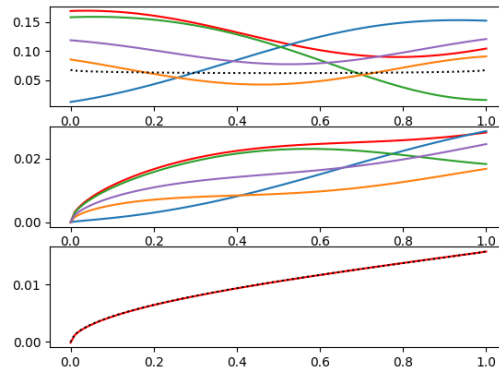
Figure 5: Heatmaps similar to Figure 4 for ICON errors for different types of in-distribution in-context examples (first label) and ICON models trained on a specific dataset (second label). Here, the question condition for the ICON prediction is the out-of-distribution optimal execution strategy  $u^*$  of the corresponding propagator model associated with hyperparameter  $\theta$ . The value of each box represents the mean error over 16 random samples of sets of hyperparameters  $\theta$  from the corresponding ranges ( $x$ -axis represents values for  $\lambda$ ,  $y$ -axis represents values for  $\beta$  and  $\gamma$ , respectively).



(a) exponential kernel



(b) non-singular power law kernel



(c) singular power law kernel

Figure 6: Illustration of the out-of-distribution prediction for  $i = 1, 2, 3$  different ICON models trained on `ode` (a), `ker` (b), `sker` (c), respectively. *Top panels:* Five selling rates  $u^{i,1}, \dots, u^{i,5}$  as in-context example conditions (colored solid lines) together with the optimal execution strategy  $u^{i,*}$  (black dashed line). *Middle panels:* The five corresponding in-context example price impact trajectories  $Y^{i,1} = \mathbf{I}_{\theta_i}(u^{i,1}), \dots, Y^{i,5} = \mathbf{I}_{\theta_i}(u^{i,5})$ . *Bottom panels:* The ICON surrogate operator prediction  $\hat{\mathbf{I}}_{\theta_i}(u^{i,*})$  (black dotted line) compared to the ground truth optimal price impact  $Y^{i,*} = \mathbf{I}_{\theta_i}(u^{i,*})$  (red solid line).

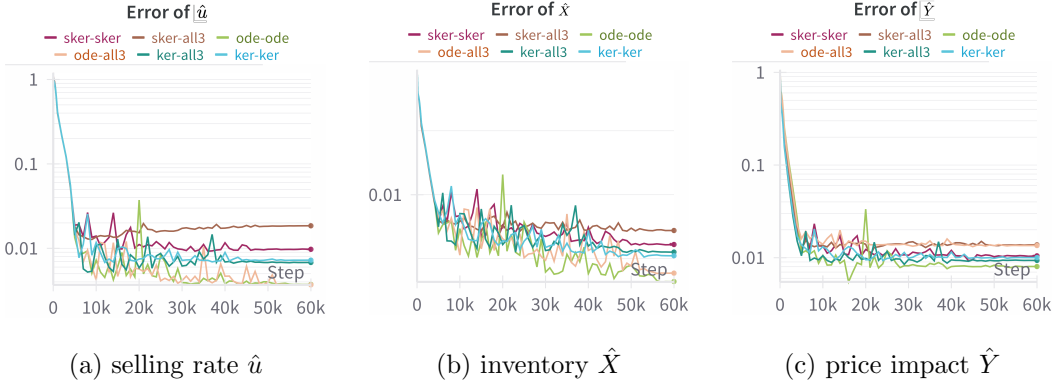


Figure 7: Relative errors of  $\hat{u}, \hat{X}, \hat{Y}$  versus training iterations for different ICON models (second label) used as surrogate operator in the optimal execution problem with a specific propagator model  $\theta$  providing the in-context examples (first label). The error values are mean values over 16 randomly selected hyperparameters  $\theta$  and initial inventories  $x$ .

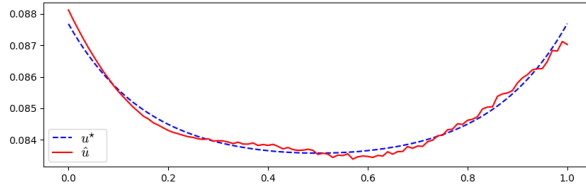
## 5 Conclusion and outlook

We introduced ICON-OCnet, a new approach to tackle an optimal (stochastic) control problem with unknown operator mapping the control to the controlled state dynamics, which is inferred from examples. To this end, we used In-Context Operator Networks (ICON), a transformer-based neural network architecture introduced in [YLMO23], enhancing data efficiency and model flexibility due to their few-shot and transfer learning capabilities. This paper provides a proof of concept of this general methodology and showcases its efficiency for finding optimal order execution strategies via in-context learning for linear propagator models. That is, using trading rates and incurred price impact trajectories as examples to learn the price impact operator (step 1), and then learn the optimal liquidation strategy based on the learned operator (step 2). The price impact environment is unknown and inferred from data prompts (context). We effectively benchmarked our approach against ground truth solutions from [AJN22]. ICON-OCnet offers rapid inference and reduced data requirements by merging offline pre-training with online few-shot learning, finding the model that is closest to the prompted examples, eliminating the need for retraining when new contexts arise.

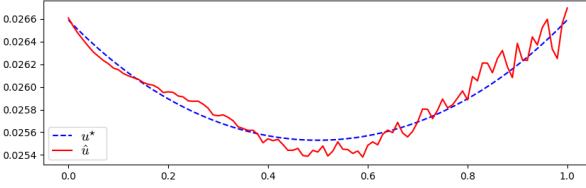
Our work paves the way for future research in several directions: First, within our examined setup, it is very conceivable to investigate (i) training ICON using real trading data, (ii) addressing more realistic non-linear price impact propagator models, including multivariate settings with cross impact, (iii) allowing for alpha signals. Moreover, regarding the downstream optimal stochastic control problem, inspired by the operator representation of the optimal execution strategy in (22), other methods such as a direct *end-to-end training* of the actual underlying *solution operator* can be explored; specifically, assessing ICON’s transfer learning capabilities to infer (near-)optimal execution strategies for non-linear propagator models from prompted optimal policies of linear models. Lastly, it is also very appealing to study our method for a broader class of stochastic optimal control problems with non-degenerate noise-driven state dynamics.

## Acknowledgement

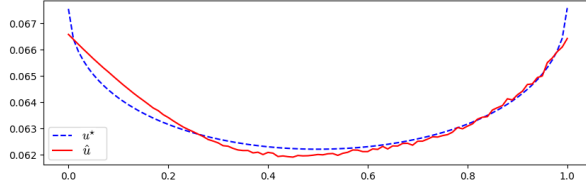
We would like to express our gratitude to Liu Yang for valuable discussions. T.M. and S.O. are supported by ONR MURI N00014-20-1-2787.



(a) exponential kernel

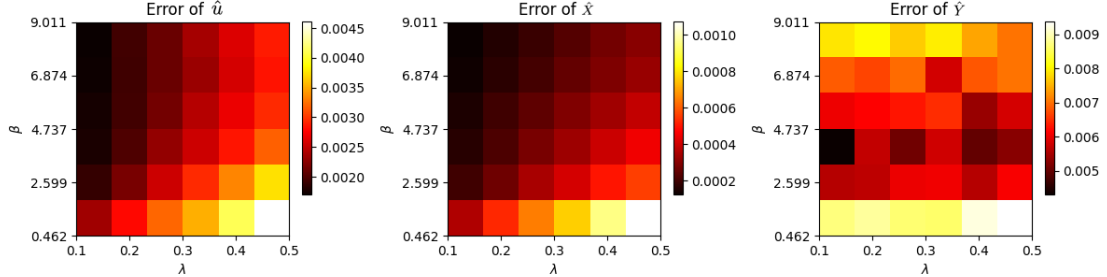


(b) non-singular power law kernel

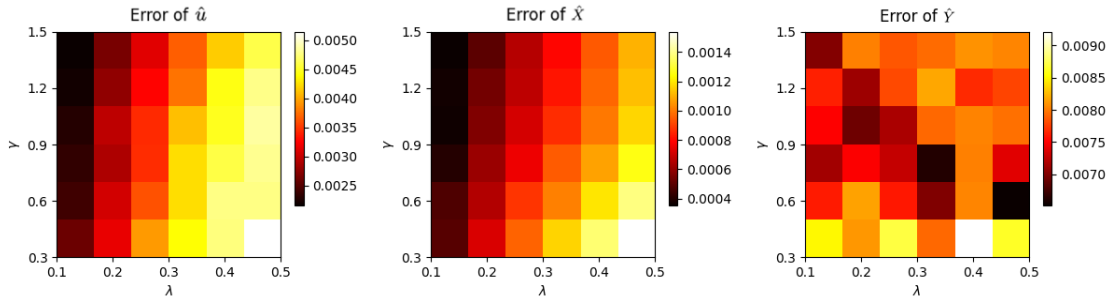


(c) singular power law kernel

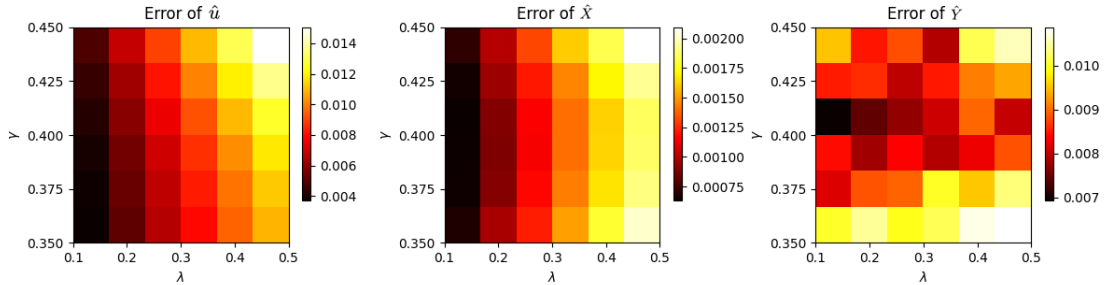
Figure 8: Example trajectories of the OCnet policy  $\hat{u}$  with corresponding  $\hat{Y}$  (red) compared to the ground truth  $u^*, Y^*$  (blue) for different propagator kernels with randomly chosen hyperparameters  $\theta$  and initial inventory  $x$ .



(a) exponential kernel

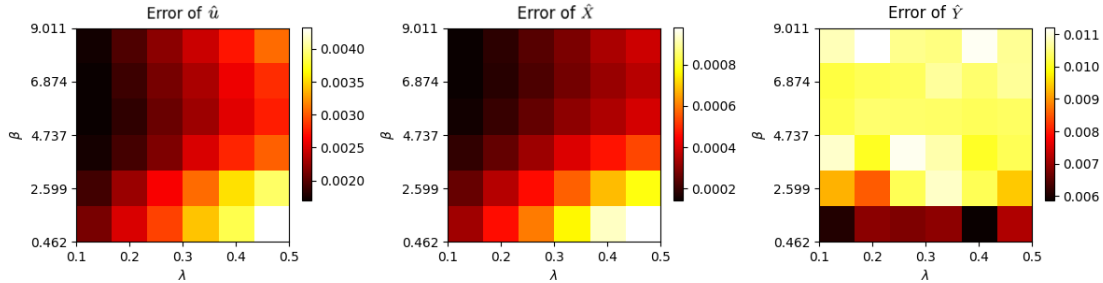


(b) non-singular power law kernel

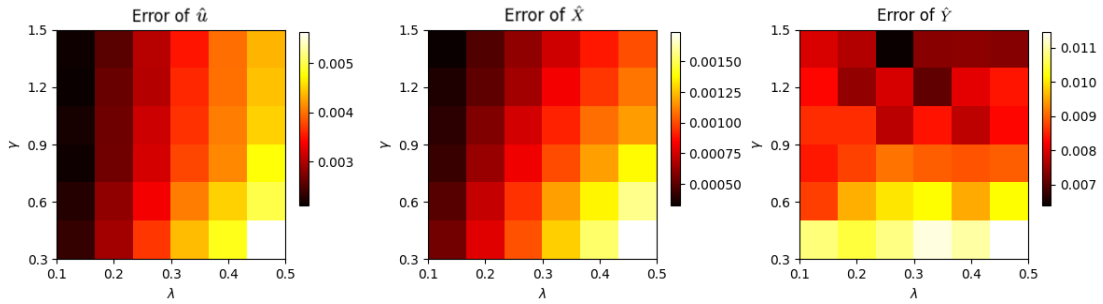


(c) singular power law kernel

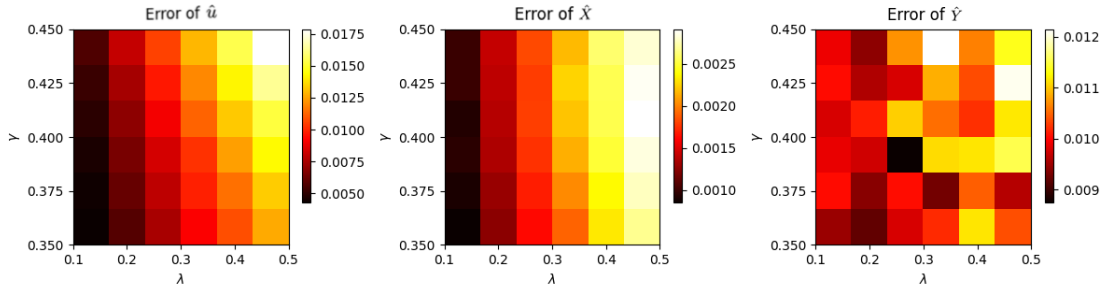
Figure 9: Heatmap for the relative error of the ICON-OCnet policy  $\hat{u}$  and corresponding controlled state processes  $\hat{X}$ ,  $\hat{Y}$  with ICON trained on a single dataset (`ode` top, `ker` middle, `scker` bottom). The prompted in-context examples for initializing ICON are in-distribution from `ode_t` (top), `ker_t` (middle), `scker_t` (bottom).



(a) exponential kernel



(b) non-singular power law kernel



(c) singular power law kernel

Figure 10: Heatmap for the relative error of the ICON-OCnet policy  $\hat{u}$  and corresponding controlled state processes  $\hat{X}$ ,  $\hat{Y}$  with ICON trained on the mixed dataset `all3`. The prompted in-context examples for initializing ICON are in-distribution from `ode_t` (top), `ker_t` (middle), `sker_t` (bottom).

## A Proof of Proposition 2.1

We apply the arguments from [AJNV23, Section 3.2] for the  $N$ -player price impact game to the present single-player setup.

First, according to the example in [AJNV23, Section 3.2] with  $N = 1$ , the objective function in (10) can be written in the form of (12) by virtue of [AJNV23, Lemma 3.1]. For the sake of clarity, we summarize the required steps here. Indeed, using integration by parts and Fubini's theorem, we can compute

$$\begin{aligned} \varrho X_T^2 &= \varrho x^2 + 2\varrho \int_0^T X_t dX_t = \varrho x^2 - 2\varrho x \int_0^T u_t dt + 2\varrho \int_0^T \left( \int_0^T u_s 1_{\{s \leq t\}} ds \right) u_t dt, \\ \phi \int_0^T X_t^2 dt &= \phi \int_0^T \left( x^2 - 2 \int_0^t X_s u_s ds \right) dt = \phi x^2 T - 2\phi \int_0^T \int_0^t \left( x - \int_0^s u_r dr \right) u_s ds dt \\ &= \phi x^2 T - 2\phi \int_0^T \int_0^t xu_s ds dt + 2\phi \int_0^T \int_0^t \left( \int_0^s u_r dr \right) u_s ds dt \\ &= \phi x^2 T - 2\phi \int_0^T xu_s(T-s) ds + 2\phi \int_0^T \left( \int_0^T 1_{\{r \leq s\}} (T-s) u_r dr \right) u_s ds. \end{aligned}$$

Consequently, we obtain

$$\begin{aligned} &\mathbb{E} \left[ \int_0^T (S_t - (\mathbf{I}_\theta(u))_t) u_t dt - \varepsilon \int_0^T u_t^2 dt - \phi \int_0^T X_t^2 dt + X_T S_T - \varrho X_T^2 \right] \\ &= \mathbb{E} \left[ \int_0^T (S_t - (\mathbf{I}_\theta(u))_t) u_t dt - \varepsilon \int_0^T u_t^2 dt + S_T x - S_T \int_0^T u_t dt \right. \\ &\quad \left. - \phi x^2 T + 2\phi \int_0^T xu_s(T-s) ds - 2\phi \int_0^T \left( \int_0^T 1_{\{r \leq s\}} (T-s) u_r dr \right) u_s ds \right. \\ &\quad \left. - \varrho x^2 + 2\varrho x \int_0^T u_t dt - 2\varrho \int_0^T \left( \int_0^T u_s 1_{\{s \leq t\}} ds \right) u_t dt \right] \\ &= \mathbb{E} [-\langle u, \mathbf{I}_\theta(u) \rangle - \langle u, \mathbf{C}(u) \rangle + \langle b, u \rangle + c] \end{aligned}$$

with  $\mathbf{C}$ ,  $b$  as defined in (13), (15), respectively, and  $c = xS_T - \phi x^2 T - \varrho x^2$ .

Next, the claim in (16) follows from the  $N$ -player game result provided in [AJNV23, Theorem 2.8] applied to the present single-player setup with objective (12) by setting  $N = 1$ ,  $\mathbf{A}_1 = \mathbf{A}_3 = 0$ ,  $\mathbf{A}_2 = \varepsilon \text{id} + \mathbf{I}_\theta + \tilde{\mathbf{C}}$ ,  $b^0 = 0$ ,  $b^i = b$ , and  $c^i = c$  therein. Moreover, note that Assumption 2.4 in [AJNV23] on  $\mathbf{A}_2$  is satisfied because  $\mathbf{I}_\theta$  in (9) with propagator kernels of type (I) and (II) is an admissible Volterra operator in the sense of [AJNV23, Definition 2.2] thanks to [AJN22, Example 2.5].

## References

- [AAB<sup>+</sup>19] Anima Anandkumar, Kamyar Azizzadenesheli, Kaushik Bhattacharya, Nikola Kovachki, Zongyi Li, Burigede Liu, and Andrew Stuart. Neural Operator: Graph Kernel Network for Partial Differential Equations. In *ICLR 2020 Workshop on Integration of Deep Neural Models and Differential Equations*, 2019.
- [AJN22] Eduardo Abi Jaber and Eyal Neuman. Optimal Liquidation with Signals: the General Propagator Case, 2022. arXiv:2211.00447.
- [AJNV23] Eduardo Abi Jaber, Eyal Neuman, and Moritz Voß. Equilibrium in Functional Stochastic Games with Mean-Field Interaction, 2023. arXiv:2306.05433.

- [BBDG18] Jean-Philippe Bouchaud, Julius Bonart, Jonathan Donier, and Martin Gould. *Trades, quotes and prices: financial markets under the microscope*. Cambridge University Press, 2018.
- [BDG24a] Fred Espen Benth, Nils Detering, and Luca Galimberti. Pricing options on flow forwards by neural networks in a Hilbert space. *Finance and Stochastics*, 28(1):81–121, 2024.
- [BDG24b] Fred Espen Benth, Nils Detering, and Luca Galimberti. Structure-informed operator learning for parabolic Partial Differential Equations, 2024. arXiv:2411.09511.
- [BFL09] Jean-Philippe Bouchaud, J. Doyne Farmer, and Fabrizio Lillo. How Markets Slowly Digest Changes in Supply and Demand. In Thorsten Hens and Klaus Reiner Schenk-Hoppe, editors, *Handbook of Financial Markets: Dynamics and Evolution*, Handbooks in Finance, pages 57–160. North-Holland, San Diego, 2009.
- [BGPW04] Jean-Philippe Bouchaud, Yuval Gefen, Marc Potters, and Matthieu Wyart. Fluctuations and response in financial markets: the subtle nature of ‘random’ price changes. *Quantitative Finance*, 4(2):176–190, 2004.
- [CJP15] Álvaro Cartea, Sebastian Jaimungal, and José Penalva. *Algorithmic and High-Frequency Trading*. Cambridge University Press, 1 edition, October 2015.
- [Gat10] Jim Gatheral. No-dynamic-arbitrage and market impact. *Quantitative Finance*, 10(7):749–759, 2010.
- [Gué16] Olivier Guéant. *The Financial Mathematics of Market Liquidity*. New York: Chapman and Hall/CRC, 2016.
- [HE16] Jiequn Han and Weinan E. Deep learning approximation for stochastic control problems, 2016. arXiv:1611.07422.
- [KKSH24] Soohan Kim, Jimyeong Kim, Hong Kee Sul, and Youngjoon Hong. An adaptive dual-level reinforcement learning approach for optimal trade execution. *Expert Systems with Applications*, 252:124263, 2024.
- [KLL<sup>+</sup>22] Nikola Kovachki, Zongyi Li, Burigede Liu, Kamyar Azizzadenesheli, Kaushik Bhattacharya, Andrew Stuart, and Anima Anandkumar. Neural Operator: Learning Maps Between Function Spaces With Applications to PDEs. *Journal of Machine Learning Research*, pages 1–97, 2022.
- [LJP<sup>+</sup>21] Lu Lu, Pengzhan Jin, Guofei Pang, Zhongqiang Zhang, and George Em Karniadakis. Learning nonlinear operators via DeepONet based on the universal approximation theorem of operators. *Nature Machine Intelligence*, 3(3):218–229, 2021.
- [NSZ23] Eyal Neuman, Wolfgang Stockinger, and Yufei Zhang. An Offline Learning Approach to Propagator Models, 2023. arXiv:2309.02994.
- [NWZ23] Marcel Nutz, Kevin Webster, and Long Zhao. Unwinding Stochastic Order Flow: When to Warehouse Trades, 2023. arXiv:2310.14144.
- [NZ23] Eyal Neuman and Yufei Zhang. Statistical Learning with Sublinear Regret of Propagator Models, 2023. arXiv:2301.05157.

- [OW13] Anna A. Obizhaeva and Jiang Wang. Optimal trading strategy and supply/demand dynamics. *Journal of Financial Markets*, 16(1):1 – 32, 2013.
- [Web23] Kevin T. Webster. *Handbook of Price Impact Modeling*. Chapman and Hall/CRC, 2023.
- [YLMO23] Liu Yang, Siting Liu, Tingwei Meng, and Stanley J. Osher. In-context operator learning with data prompts for differential equation problems. *Proceedings of the National Academy of Sciences*, 120(39):e2310142120, 2023.